High variability of dissolved iron concentrations in the vicinity of Kerguelen Island (Southern Ocean)

F. Quéroué[1,2,3,4], G. Sarthou[2], H.F. Planquette[2], E. Bucciarelli[1,2], F. Chever[2], P. van der Merwe[4], D. Lannuzel[3,4], A.T. Townsend[5], M. Cheize[2], S. Blain[6,7], F. d'Ovidio[8] and A.R. Bowie[3, 4]

[1] Université de Bretagne Occidentale, Brest, 29200, France

[2] LEMAR-UMR 6539, CNRS-UBO-IRD-IFREMER, Place Nicolas Copernic, 29280 Plouzané, France

[3] Institute for Marine and Antarctic Studies, University of Tasmania, Hobart, Tas 7001, Australia

[4] Antarctic Climate & Ecosystems Cooperative Research Centre, University of Tasmania, Hobart, Tas 7001, Australia

[5] Central Science Laboratory, University of Tasmania, Hobart, Tas 7001, Australia

[6] Laboratoire Océanographie Biologique de Banyuls sur Mer, Université Pierre et Marie Curie, Paris 06, quai Fontaulé, 66650 Banyuls sur Mer, France

[7] Laboratoire Océanographie Biologique de Banyuls sur Mer, CNRS, Paris 06, quai Fontaulé, 66650 Banyuls sur Mer, France

[8] Sorbonne Universités (UPMC, Univ Paris 06)-CNRS-IRD-MNHN, LOCEAN-IPSL, 4 place Jussieu, 75005 Paris, France

Correspondence to: G. Sarthou (Geraldine.Sarthou@univ-brest.fr)

Abstract

Dissolved Fe (dFe) concentrations were measured in the upper 1300 m of the water column in the vicinity of Kerguelen Island as part of the second KErguelen Ocean Plateau compared Study (KEOPS2). Concentrations ranged from 0.06 nmol L^{-1} in offshore, Southern Ocean waters, to 3.82 nmol L^{-1} within Hillsborough Bay, on the north-eastern coast of Kerguelen Island. Direct island runoff, glacial melting and resuspended sediments were identified as important inputs of dFe that could potentially fertilise the northern part of the plateau. A significant deep dFe enrichment was observed over the plateau with dFe concentrations increasing up to 1.30 nmol L^{-1} close to the seafloor, probably due to sediment resuspension and pore water release. Biological uptake was shown to induce a significant decrease in dFe concentrations between two visits (28 days apart) at a station above the plateau. Our work also considered other processes and sources, such as lateral advection of enriched seawater, remineralization processes and the influence of the polar front (PF) as a vector for Fe transport. Overall, heterogeneous sources of Fe over and off the Kerguelen Plateau, in addition to strong variability in Fe supply by vertical or horizontal transport, may explain the high variability in dFe concentrations observed during this study.

1 Introduction

Iron (Fe) has been shown to be an essential trace metal controlling phytoplankton growth and primary production in about 50% of the World's oceans (Moore et al., 2001) including high nutrient low chlorophyll (HNLC) regions. The main sources of Fe in the World's oceans are atmospheric deposition (wet or dry) (e.g. Jickells et al., 2005), sediment resuspension and pore water release (e.g. Elrod et al., 2004; Lam and Bishop, 2008), hydrothermal activity (Tagliabue et al., 2010), and remineralization of organic matter (Ibisanmi et al., 2011). In the Southern Ocean, dust inputs have been considered to be small due to its remoteness from land masses (Wagener et al., 2008; Heimburger et al., 2013), but the other sources of Fe were shown to induce natural fertilisation in several sites including the Crozet Plateau (Pollard et al., 2009; Planquette et al., 2011), the Scotia Sea (Dulaiova et al., 2009; Ardelan et al., 2010; Nielsdóttir et al., 2012; Hatta et al., 2013; Measures et al., 2013), the Ross Sea (Smith Jr et al., 2012) and the Kerguelen Plateau (Blain et al., 2007; Blain et al., 2008), all stimulating phytoplankton blooms and enhancing carbon sequestration with varying magnitudes.

During the first Kerguelen Ocean Plateau compared Study (KEOPS1) held in late austral summer 2005, the impact of natural fertilisation on primary productivity and carbon export was demonstrated in this area (Blain et al., 2007; Savoye et al., 2008). The surface area of the observed phytoplankton bloom was about 45,000 km^2 and led to a carbon sequestration efficiency 18 times higher (Chever et al., 2010) than estimated around Crozet Islands (bloom area 90,000 km^2) during the CROZEX experiment in the same year (Pollard et al., 2009; Morris and Charette, 2013). A second cruise, KEOPS2 (Kerguelen Ocean and Plateau compared Study 2) was designed to study the development of the Kerguelen bloom in early spring 2011 and in the offshore fertilisation area further east. In this paper, we present dissolved Fe (dFe) concentrations clustered into 5 groups (near-coastal, plateau, recirculation, north of the polar front (PF), HNLC area) and discuss their distributions in relation to potential new and regenerated sources. Where possible, an estimate of the biological uptake of Fe is provided. Finally, dFe data presented in this paper together with particulate Fe data from a closely aligned companion study (van der Merwe et al., 2015) are combined by Bowie et al. (2014) in order to establish short-term Fe budgets at three sites (above the Plateau, in the recirculation area, and the HNLC area).

2 Materials and Methods

2.1 Study Area

During austral spring (7/10/2011 - 30/11/2011), 149 seawater samples from 15 stations were collected as part of the KEOPS2 oceanographic research cruise (Fig. 1, Table 1) in the vicinity of Kerguelen Island in the Southern Ocean (48.40S – 50.62°S and 66.68°E-74.65°E). Two stations were sampled over the plateau (A3 and G-1), south of the island. A3 was visited twice, 28 days apart, in the early stage and during the build up of the spring phytoplankton bloom. An East-West (E-W) transect (from TEW-1 to F-L) was sampled from the Kerguelen coast to offshore waters, and crossed the PF twice. Finally, three additional stations were analyzed within a complex system of recirculation located in a stationary meander of the PF (E-3, E-4W-2 and E-5). An open ocean station (R-2), was located in the HNLC area south-west of Kerguelen Island and south of the PF.

2.2 Sampling and analytical methods

Cleaning, sampling, handling and processing of the samples were conducted using stringent trace metal clean protocols as recommended by the GEOTRACES program (Cutter et al., 2010; Cutter, 2013). Samples were collected using a trace metal clean rosette (TMR, model 1018, General Oceanics) equipped with twelve 10 L externally closing Teflon-lined Niskin-1010X bottles mounted on a polyurethane powder-coated aluminium frame especially designed for trace metal work (Bowie et al., 2009). Seawater was sub-sampled for dFe via a Teflon tap connected to acid cleaned 0.2 μm filter cartridges (Pall Acropak® and Sartorius Sartrobran® 300). Acid cleaned low density polyethylene bottles (60 mL) were rinsed 3 times with ~ 20 mL of seawater before final sample collection. Dissolved Fe samples were acidified to pH ~ 2 using concentrated ultrapure hydrochloric acid (Seastar Baseline, HCl). The sample bottles were then double bagged and stored at ambient temperature in the dark until analysis. The shallowest sample was collected at 15 m depth in order to avoid contamination from the ship. Samples were collected off plateau to a depth of 1300 m.

Dissolved Fe was analysed on board at least 24 h after collection by flow injection analysis (FIA) with online solid phase extraction onto 8-hydroxyquinoline (8-HQ) resin and chemiluminescence detection, following a method adapted from Obata et al. (1993) (Sarthou et al., 2003). All analyses were conducted inside a class 100 laminar flow hood within a containerised clean laboratory, using high-efficiency particulate air (HEPA) filters. During the cruise, hydrogen peroxide, ammonium acetate buffer and HCl blanks were consistently below the detection limit (0.017 ± 0.012 nmol L^{-1}, n = 22), and therefore, the system was deemed suitable for open ocean seawater analysis (Johnson et al., 2007). Each sample was analysed in triplicate with an average precision of 4.8 % (n = 149). The North Pacific SAFe Surface (SAFe S) (0.094 ± 0.003 nmol L^{-1}, n = 3) and SAFe Deep D2 (0.95 ± 0.05 nmol L^{-1}, n = 3) reference samples were measured for dFe and the results were in excellent agreement with the consensus values (S1 = 0.095 ± 0.008 nmol L^{-1} and D2 = 0.96 ± 0.02 nmol L^{-1}; Johnson et al., 2007).

Potential temperature (Θ), salinity (S), oxygen (O_2) and beam attenuation data were retrieved from the CTD sensors. We used the data from the CTD casts that were deployed immediatly before or after our TMR casts.

3 Results and discussion

3.1 Clustering of stations

The presentation and discussion of results are organised by clusters, which were defined considering the hydrography and the complex regional circulation. Water masses were identified using Θ-S diagrams (Fig. 2).

Cluster 1 includes TEW-1 and TEW-2 stations located at the north eastern flank of Kerguelen Island and North of the PF, with shallow waters (~ 85 m bottom depth), low salinity (33.6–33.8) and low density anomaly (< 27.0 kg m^{-3}). Below the surface mixed layer (SML), the water masses can be defined as subsurface (shelf) waters.

Cluster 2 includes stations located above the central part of the Kerguelen Plateau (A3-1, A3-2, G-1, and TEW-3, bottom depths lower than 600 m), and located south of the PF, with a

minimum of temperature around 200 m. At A3-1, stratification had not yet started and surface water temperature was low (~ 1.7 °C) and typical of winter conditions. Stations A3-2 and G-1 presented similar water masses (Fig. 2). The SMLs were observed down to 125 m and 65 m, respectively. Below, Winter Water (WW) is encountered with temperatures around 1.7 °C at 225 m and 115-210 m, respectively. The inclusion of TEW-3 in cluster 2 is debatable given its location at the plateau edge. Indeed, although TEW-3 can be considered as south of the PF, its location within the polar front Jet is likely more correct. However, a structure comparable to A3-1, A3-2 and G-1 was observed below the surface waters with a WW temperature just below 2 °C.

East of Kerguelen plateau, the PF presents a permanent meander (Park et al., 2014). This meander delimits a region with a complex circulation including stations TEW-4, E-2, TEW-5, E-3, E-4W-2, and E-5), and is defined as cluster 3. All these stations showed very similar Θ-S profiles (Fig. 2). The warmest sea surface temperatures were observed at station E-5, due to the decrease in the mixed layer depth (MLD) and progression into summer. Below the surface water (SW), a subsurface temperature minimum (~ 1.7-1.8°C) was observed between 170 m and 220 m, characteristic of the WW (Fig. 2). Below, the oxygen minimum around 600-800 m (175 μmol kg^{-1}) can be attributed to the Upper Circumpolar Deep Water (UCDW). Deeper in the water column (below 1300 m), the salinity increased towards a salinity maximum (~ 34.75) indicating the presence of the Lower Circumpolar Deep Water (LCDW).

Stations TEW-7 and F-L (cluster 4), located north of the PF and east of the Plateau presented the warmest surface waters of the study (4.2°C) characteristic of the Sub-Antarctic Surface Water (SASW). The Antarctic Intermediate Water (AAIW) occurred deeper, at 170 m (TEW-7) and 290 m (F-L) (Fig. 2). Below the AAIW, the UCDW and the LCDW were encountered.

Station R-2, located in the HNLC area, stands on its own in cluster 5. A salinity minimum (33.78) and a surface temperature maximum (2.0°C) were observed in the upper 100 m, which is characteristic of the SW (Fig. 2). At 200 m, the temperature minimum (1.6°C) was indicative of WW. The oxygen minimum (170 μmol kg^{-1}) defined the upper circumpolar deep water (UCDW). Deeper in the water column (below 1300 m), the salinity increased towards a salinity maximum (~ 34.73) indicating the presence of the lower circumpolar deep water (LCDW).

3.2 A general overview of dFe distributions

Median dFe concentrations for the different water masses and clusters (2 to 5) are plotted on Fig. 3.

In the surface waters, near-coastal stations presented the highest concentrations (2.10 ± 0.77 nmol L^{-1}). When considering the other stations, the lowest sea-surface concentrations were found at station R-2 (0.09 ± 0.01 nmol L^{-1}), while the highest were observed in cluster 4 (0.26 ± 0.09 nmol L^{-1}). If we compare our results in the surface waters to the dataset compiled by Tagliabue et al. (2012), R-2 had lower values than the mean value of the Indian-Antarctic zone (0.43 ± 0.51 nmol L^{-1}), whereas the mean value in cluster 4 was higher than the mean value of the Indian-Subantarctic zone (0.23 ± 0.20 nmol L^{-1}). Tagliabue et al. (2012) suggested that the higher mean surface value in the Antarctic than in the Subantarctic zone could be due to a lower biological activity in the former. In our study, the biological activity was much lower at station R-2 (Antarctic zone) than in cluster 4 (Subantarctic zone). Indeed the highest integrated concentrations over 200 m for chlorophyll-*a* (Chl-*a*) were observed in cluster 4 (223 mg m^{-2} – 354 mg m^{-2}) (Lasbleiz et al., 2014). So, the lower dFe value at R-2 compared to cluster 4 might not reflect differences in biological activity but, rather, in Fe inputs (see below).

At intermediate depths, median dFe were not significantly different among clusters 2, 3, and 5 in the WW (ANOVA, F=0.54, p=0.5904), suggesting that the whole area presented similar dFe concentrations at the surface during winter time. In cluster 4, dFe in the AAIW presented relatively high values (0.46 ± 0.06 nmol L^{-1}), consistent with the high dFe values in the surface waters of the Antarctic zone (Tagliabue et al., 2012).

In the deep waters (LCDW and UCDW), stations above the Plateau were enriched with Fe compared to all other clusters. When considering the clusters in offshore waters, values for stations in cluster 4 (0.57 ± 0.04 nmol L^{-1}) were significantly higher than those in clusters 3 (0.41 ± 0.09 nmol L^{-1}, Mann Whitney, W=3.0, p=0.0007) and in cluster 5 (0.33 ± 0.02 nmol L^{-1}, Mann Whitney, W=45.0, p=0.003). This is consistent with the compilation by Tagliabue et al. (2012), which showed that deep values were higher in the Subantarctic zone than in the Antarctic zone (0.64 ± 0.31 nmol L^{-1} and 0.51 ± 0.24 nmol L^{-1}, respectively). This difference was attributed to both higher ligand concentrations at depth (Thuróczy et al., 2011) and deep

184 Fe inputs such as hydrothermal activity, with the greatest input in the Indian Subantarctic
185 region (Tagliabue et al., 2012).

186

187 ### 3.3 Coastal area (cluster 1)

188 TEW-1 and TEW-2 stations were sampled on the same day in order to provide a nearshore
189 data set of dFe. Stations TEW-1 and TEW-2 were in shallow waters approximately 10 and 75
190 kms away from Hillsborough Bay coast, respectively.
191 Median profiles of dFe, with minimum and maximum values in this cluster, are shown on Fig.
192 4a. At station TEW-1, dFe concentrations were high (> 1.8 nmol L^{-1}, Table 1), and increased
193 steadily from 15 m depth (1.82 nmol L^{-1}) to 50 m depth (2.58 nmol L^{-1}). Close to the seafloor
194 a sharp increase at 62 m depth (3.82 nmol L^{-1}) was measured. These are the highest values
195 measured during this study. At TEW-2, dFe concentrations were lower than at TEW-1,
196 increasing from 1.26 nmol L^{-1} in surface waters to 1.82 nmol L^{-1} at 62 m depth.
197 Several studies have already measured dFe at near-coastal stations in the Southern Ocean
198 (Table 2). Around Kerguelen (KEOPS1), around Crozet (CROZEX), and around South
199 Shetland Island, dFe concentrations were within the same order of magnitude as the present
200 study (~ 2-4 nmol L^{-1}; Table 2). During ANTARES3 (Kerguelen), dFe concentrations were 5
201 to 10 fold higher (22.6 nmol L^{-1}). This discrepancy was already discussed (Blain et al., 2008)
202 and is likely partly due to methodological differences (0.4 μm filtration, nitric acid
203 acidification and 2-year storage).

204 The elevated dFe concentrations observed at near shore sites are most certainly indicative of
205 Fe sourced from the islands; a feature clearly evident during the present study and illustrated
206 in Fig. 5. This source is most likely a combination of direct island runoff, glacial melt and
207 resuspended sediments. High particle loads (as estimated by beam attenuation data) were
208 encountered throughout the water column of TEW-1 and TEW-2, with higher concentrations
209 at TEW-1, especially at 10 m depth and close to the seafloor (Fig. 6). Low salinities (33.63 ±
210 0.01, n=61) were also measured at TEW-1, which corroborates our hypothesis of direct island
211 runoff and/or glacial melt inputs. Moreover, the Ampère Glacier which is the largest glacier
212 from the Cook icecap (about 500 km^2), thins rapidly over the last decade (Berthier et al.,

2009), especially towards the east of the icecap, up to 1.5 m per year. This discharge includes small basalt-derived particles (Frenot et al., 1995) and could partially discharge in Hillsborough Bay (Y. Frenot, pers. comm.). Finally, TEW-1 showed the highest lithogenic silica (LSi) concentrations of the study area (1.31 ± 0.14 µmol L^{-1}; Closset et al., 2014; Lasbleiz et al., 2014) and TEW-2 showed slightly lower LSi concentrations (0.54 ± 0.02 µmol L^{-1}). Gradients in LSi and dFe are probably indicative of glacial melt inputs, Fe being leached from nanoparticulate Fe (oxyhydr)oxides present in glacial rock flour (Raiswell et al., 2010; Raiswell, 2011) and LSi being weathered from silicate rich minerals (SiO_2, Doucet et al., 2005).

Sedimentary inputs (e.g. Johnson et al., 1999; Elrod et al., 2004; Chase et al., 2005; Lam et al., 2006; Planquette et al., 2011; Homoky et al., 2013; Marsay et al., 2014) could also explain the increased dFe concentrations encountered at both stations close to the seafloor (3.82 and 1.82 nmol L^{-1} at stations TEW-1 and TEW-2, respectively). Unfortunately, particulate Fe (pFe) concentrations were not measured at these near-coastal locations to confirm sediment resuspension, but the fact that the beam attenuation increased close to the seafloor of station TEW-1 (Fig. 6) and that high dMn concentrations at TEW-1 (5.40 nmol L^{-1}) and TEW-2 (1.92 nmol L^{-1}) were also measured (Quéroué et al., unpublished data) strongly supports this hypothesis.

Dissolved Fe concentrations in the water column may not only reflect sedimentary inputs but also inputs from remineralization processes. However, since deciphering remineralization from sedimentary inputs at shallow stations is difficult, remineralization process will only be discussed for clusters 3, 4, and 5.

3.4 Central Plateau area (cluster 2)

Similar dFe vertical profiles were observed at A3-2, G-1, and TEW-3 with low dFe concentrations at the surface (~ 0.1-0.2 nmol L^{-1}), increasing towards the bottom, up to 1.30 ± 0.01 nmol L^{-1}, 0.99 ± 0.01 nmol L^{-1}, and 0.37 ± 0.00 nmol L^{-1}, respectively (Table 1). Median profiles of dFe, with minimum and maximum values in this cluster, are shown on Fig. 4b. At

241 station A3-1, concentrations were higher in the SML (~ 0.3-0.4 nmol L^{-1}), then increased with
242 depth below the SML up to 0.40 ± 0.01 nmol L^{-1} at 350 m.

243 Over the Kerguelen Plateau, 24 shelf stations have been investigated during several cruises
244 (Table 2). The highest concentrations were measured during ANTARES3 (~ 6 nmol L^{-1}) in
245 the northern part of the Kerguelen Plateau at a station located 76 km away from the shore
246 (Station K4, 40 m). The lowest concentrations were measured during KEOPS1 (0.05
247 nmol L^{-1}) within the top 200 m of water. Above 100 m, lower concentrations were observed
248 during KEOPS1 compared to KEOPS2 (Table 2). This can be explained by a more advanced
249 phytoplankton bloom during KEOPS1 (summer conditions) than KEOPS2 (spring
250 conditions). In surface waters, dFe concentrations measured during KEOPS2 were of similar
251 magnitude than those measured in the vicinity of the South Shetland Islands (Nielsdóttir et al.,
252 2012, Table 2).

253 A deep Fe-enriched reservoir was also observed above the Kerguelen Plateau during KEOPS1
254 (Blain et al., 2008; Chever et al., 2010). Non reductive dissolution of resuspended sediments
255 is a potentially important source of dFe as observed at near-coastal stations (e.g. Homoky et
256 al., 2013). At station A3, high LSi concentrations (1.34 ± 0.07 µmol L^{-1}; Lasbleiz et al., 2014)
257 were observed just above the seafloor in the benthic boundary layer (BBL), also suggesting
258 sedimentary inputs. This is corroborated by high pFe values at A3-1 and A3-2 (30 and 15
259 nmol L^{-1} respectively) and pFe:pAl ratios that resemble basalt over the Kerguelen Plateau
260 (van der Merwe et al., 2015).

261 The variability of the deep dFe concentrations above the Plateau may be due to variability in
262 sedimentary inputs in this highly dynamic region. All stations from this cluster except station
263 TEW-3 had high beam attenuation values close to the seafloor, which most likely indicates
264 the presence of resuspended particles at these depths (98% for TEW-3 vs. 92-97% for the
265 other three stations, Fig. 6). Marsay et al. (2014) performed a very detailed sampling of near-
266 bottom waters for dFe over the Ross Sea shelf and showed that dFe concentrations displayed
267 a quasi-exponential increase with depth, with a pronounced gradient towards the sea-floor.
268 When plotting our dFe data as a function of height above the seafloor, we also observed an
269 exponential increase with depth (Fig. 7). Clearly, at station TEW3, the least pronounced
270 gradient between dFe vs. height above seafloor was observed.

Hydrothermal input may be an additional Fe source above the Kerguelen Plateau, more particularly in the vicinity of the Heard Island. The Mn:Al ratio at this station is much lower than any of the other stations 0.007-0.009 (van der Merwe et al., 2015) and very similar to the Kerguelen Island Basalt mean of 0.004-0.010 (Gautier et al., 1990). This supports fresh weathering of basalt downstream of A3, which may be glacial/fluvial runoff or hydrothermal.

Diffusion from pore waters is another important possible source of Fe for the BBL (Elrod et al., 2004). When sediment receives large amount of organic carbon, it is covered by a fluff layer composed mainly of broken cells, as observed during KEOPS1 for stations above the Plateau (Armand et al., 2008). Diagenesis then produces suboxic/anoxic conditions, which are key conditions to mobilize Fe because of the high solubility of the reduced Fe(II) form (Walsh et al., 1988). Anoxic conditions were observed 2 cm below the sediment surface at the A3 stations (P. Anschutz. pers. comm.) suggesting that, in pore waters above the plateau, Fe could be in the reduced form and diffuse into the bottom water column.

For all stations in cluster 2, dFe minima were observed in the SML, which could reflect biological uptake and/or particle scavenging. A significant decrease was observed in dFe concentrations in the SML between A3-1 (0.33 ± 0.06 nmol L^{-1}) and A3-2 (0.15 ± 0.02 nmol L^{-1}) (t-test, $p<0.05$). The first visit to site A3 (A3-1, 20 October) was characteristic of early bloom conditions, while during the second visit 28 days later (A3-2, 17 November), chlorophyll-a concentrations at the sea-surface increased by about three-fold as a consequence of a large diatom bloom (Fig. 6c) (Lasbleiz et al., 2014). Moreover, based on the beam attenuation profiles, A3-2 seemed to have more particles (likely of biogenic origin) than A3-1 within the top 200 m. This is confirmed by the fact that at these depths, the Fe:Al ratio at A3-2 is higher than A3-1 and in all cases, well above the crustal ratios. This may indicate that more pFe of biogenic origin was present at A3-2 than at A3-1 (van der Merwe et al., 2015), and confirm an increased biological uptake at A3-2 compared to A3-1. Between the two visits, integrated dFe concentrations over 200 m decreased (62.6 µmol m^{-2} vs. 28.1 µmol m^{-2}), while concentrations of particulate organic carbon (POC) (from 1259 to 2267 mmolC m^{-2}) increased (Lasbleiz et al., 2014). The decrease in dFe stock represents ~ 35% of the winter stock, defined as the dFe concentration in the WW (0.51 nmol L^{-1}) multiplied by the depth of the temperature minimum (200 m) (Blain et al., 2007). Taking into account the decrease in

dFe stock and the increase in POC stock, the Fe:C ratio of the biomass that developed between the two visits at A3 can be estimated to equal 34 μmol mol^{-1}, a ratio consistent with literature values for diatoms in Fe-replete waters of the Southern Ocean (Sunda and Huntsman, 1995; Sunda, 1997;Twining et al., 2004; Sarthou et al., 2005). Although this is a rough estimate which does not take into account any additional inputs or removal processes, this result indicates that the dFe decrease between A3-1 and A3-2 could be due, at least partly, to biological uptake.

3.5 Recirculation area (cluster 3)

Median profiles of dFe, with minimum and maximum values in this cluster, are shown on Fig. 4c. A two-way ANOVA, based on depth and location (i.e. station), showed that location had a significant effect on dFe variability ($F=24.92$, $df=5$, $P<0.01$). It defined five homogeneous groups from the 6 stations tested (E-2/E-5, E-5/TEW-4, TEW-4/TEW-5, TEW-5/E-4W-2, and E-3), showing the strong variability of vertical dFe distributions in this cluster. Stations E-2 and E-5 showed very low concentrations near the sea-surface (from 0.06 nmol L^{-1} to 0.10 nmol L^{-1}) and a gradual increase with depth (~ 0.37-0.39 nmol L^{-1}, at 1300 m) (Table 1). A dFe maximum was observed at intermediate depths (500-600 m, 0.34-0.43 nmol L^{-1}). The dFe profile at station TEW-4 is homogeneous below 150 m. The dFe maximum at 600 m is 0.39 nmol L^{-1} and, at 1300 m, dFe reaches 0.42 nmol L^{-1}.

Concentrations at stations TEW-5 and E-4W-2 were close to those at stations TEW-4 in the upper 150 m (0.11-0.22 nmol L^{-1}), but these stations showed higher concentrations at intermediate depths (150-200 m, 0.21-0.30 nmol L^{-1}). Below 150-200 m, concentrations reached values of ~ 0.4 nmol L^{-1}, except for the deepest value at station E-4W-2 (0.61 ± 0.02 nmol L^{-1}, 1100 m). This sampling depth was located less than 200 m away from the seafloor and was associated with an increase in beam attenuation (see Fig. 6), which indicated a high number of particles and potential sedimentary inputs.

Station E-3 had high surface dFe concentrations at 40 m (0.38 ± 0.03 nmol L^{-1}) followed by a minimum at 100 m (0.22 ± 0.01 nmol L^{-1}) (Table 1). A subsurface dFe maximum was

329 observed at intermediate depth (300 m, 0.50 ± 0.01 nmol L^{-1}) while concentrations remained
330 homogenous at deeper depths (0.52 ± 0.01 nmol L^{-1}).

331 In this cluster, dFe concentrations were comparable to concentrations measured at stations off
332 Crozet plateau that were not under HNLC conditions (Planquette et al., 2007). However
333 during KEOPS2, water column dFe concentrations were lower than those observed during
334 ANTARES 3 and in the South Shetland Islands sites, most likely due to the greater distance
335 of the KEOPS2 stations from the shore (Table 2).

336 The higher sea-surface dFe concentrations at stations TEW-4, E-4W-2, and E-3, may be
337 indicative of atmospheric inputs. However no particulate aluminium (pAl, a proxy for
338 atmospheric inputs) surface enrichment in the recirculation area was observed during the
339 study (van der Merwe et al., 2015), suggesting that air-masses were not carrying enough
340 aerosols to enhance pAl surface concentrations. Moreover, Bowie et al. (2014) showed that
341 atmospheric inputs were in the order of 50 nmol m^{-2} d^{-1} which is insignificant compared to the
342 lateral supply of dFe in the same area 180-2400 nmol m^{-2} d^{-1}). Significant ^{224}Ra and ^{223}Ra
343 activities were detected in offshore waters south of the PF (Sanial et al., 2015). These
344 observations clearly indicated that dissolved sediment-derived inputs of Ra can be rapidly
345 transferred towards offshore waters. These Ra-enriched waters could also be enriched with
346 dissolved sediment-derived Fe.

347 Within the waters characterised by an oxygen minimum, remineralization of sinking organic
348 matter may exert a primary control on dFe distribution. To assess this hypothesis, we looked
349 at the relationship between dFe and the apparent oxygen utilisation (AOU), from the start of
350 the oxycline (~ 150-200 m) to the bottom of the UCDW (700-1100 m). In these waters, the
351 AOU indicates the amount of oxygen that has been consumed during remineralization since
352 the waters left the surface, whereas dFe concentration equals the preformed dFe plus any dFe
353 released from remineralization, minus any dFe scavenged by particles (Hatta et al., 2014).
354 Dissolved Fe concentrations showed a significant positive correlation with the AOU for all
355 the stations in the recirculation area (ANOVA, $p < 0.01$), meaning that remineralization was
356 likely a significant source of dFe at these depths. Station E-3 clearly presented a different
357 behaviour compared to the other stations of cluster 3 (Fig. 8). Indeed, although the slopes
358 were not significantly different (0.0016 ± 0.0003 mmol mol^{-1} for E-3 and 0.0018 ± 0.0002

359 mmol mol^{-1} for all stations except E-3, ANOVA, $p > 0.1$), the intercepts were different (0.26
360 ± 0.05 nmol L^{-1} for E-3 and 0.08 ± 0.03 nmol L^{-1} for all the other stations, ANOVA, $p <$
361 0.01). This suggests that a pre-formed dFe signal was present at E-3, which could explain the
362 highest dFe values observed at this station. Using this slope of the dFe:AOU relationship and
363 a modified oxygen consumption ratio of 1.6 moles O_2 per mole of carbon remineralized
364 (Martin et al., 1987), a net Fe:C ratio for the remineralization process equal to 2.6-2.9 µmol
365 mol^{-1} was estimated. This ratio is very similar to Fe:C ratios of Fe-limited diatoms from
366 culture studies and in-situ Southern Ocean data (Martin et al., 1987; Sunda, 1997; Sarthou et
367 al., 2005).

368

369 ### 3.6 North polar front stations (cluster 4)

370 Stations TEW-7 and F-L were located northeast of the PF, approximately 270 and 313 km
371 northeast of Kerguelen Island with bottom depths of 2500 m and 2700 m, respectively. These
372 stations presented comparable vertical profiles (Fig. 4d). In the upper 50 m, dFe
373 concentrations were depleted at 0.22 and 0.17 nmol L^{-1} (at 40 m at station TEW-7, and 35 m
374 at station F-L, respectively) and then gradually increased within the mesopelagic zone to
375 finally reach 0.59 nmol L^{-1}at 1300 m depth (Station TEW-7) and 0.67 nmol L^{-1} at 1000m
376 depth (Station F-L).
377 During ANTARES 3, station K14, which was also sampled northeast of the PF, exhibited
378 high values at the surface (4.11 nmol L^{-1} at 40 m depth). This was interpreted as the result of a
379 mixing between SASW and water masses coming from the West and enriched by sweeping
380 the plateau (Bucciarelli et al., 2001), at a time when no significant sink occurred (beginning of
381 spring, ~ 0.4 µg L-1 of Chl-*a*).

382 During KEOPS2, however, the decrease in dFe concentrations within the SASW, around 35-
383 40 m depth, can result from biological uptake. This is suggested by the high biomass reported
384 at stations TEW-7 and F-L (Lasbleiz et al., 2014), with the highest integrated concentrations
385 over 200m for Chl-*a* (> 220 mg m^{-2}), biogenic silica (> 300 mmol Si m^{-2}), particulate organic
386 carbon (> 1200 mmol C m^{-2}), particulate organic nitrogen (> 200 mmol N m^{-2}), and
387 particulate organic phosphorus (> 30 mmol P m^{-2}). This biological uptake is also reflected in

388 the composition of suspended particles (van der Merwe et al., 2015). In surface waters, higher
389 pFe:pAl elemental ratios were observed compared to those from the base of the SML, which
390 is indicative of a conversion of dFe into biogenic pFe. However, compared to the less
391 productive recirculation area (see section 3.5), the surface dFe concentrations are higher by
392 0.1 nmol L^{-1}. This could be explained by the fact that, like during ANTARES 3, a portion of
393 the water masses found at TEW-7 and F-L likely interacted more with both the plateau and
394 shallow coastal waters of Kerguelen Island than the water masses from the recirculation area.
395 This hypothesis is supported by the general circulation in this region (Park et al., 2014) that
396 shows that water masses are carried northwards between the island and the recirculation area
397 and finally looped back East of the recirculation area. A Lagrangian model of Fe transport
398 based on altimetry (d'Ovidio et al., 2014) also confirms that the waters at F-L and TEW-7 are
399 mainly coming from the northern part of plateau. Moreover, close to the seafloor, van der
400 Merwe et al. (2015) observed high values of pFe, pMn, and pAl, likely due to sediment
401 resuspension.

402 As for the recirculation area, dFe concentrations in the mesopelagic zone may also reflect
403 remineralization processes. Dissolved Fe concentrations present a significant positive
404 relationship with AOU for both stations ($dFe = 0.0014 \pm 0.0003 \times AOU + 0.32 \pm 0.03$, $n = 5$,
405 $r^2 = 90\%$, $p < 0.05$, and $dFe = 0.0020 \pm 0.0005 \times AOU + 0.24 \pm 0.07$, $n = 7$, $r^2 = 74\%$, $p <$
406 0.05 for stations TEW-7 and F-L, respectively). The two slopes are not significantly different
407 (ANOVA, $p > 0.1$). When combining the two data sets (Fig. 8), the slope is also not
408 significantly different from the slope in the recirculation area (ANOVA, $p > 0.1$), suggesting
409 that Fe and C are remineralized at the same rates in both regions (Fe:C ~ 2 μmol mol^{-1}).
410 However, the intercept is significantly different from the intercept of the recirculation area
411 (without the station E-3, see above) and from zero (ANOVA, $p < 0.01$), suggesting the
412 presence of preformed Fe in these waters.

413

3.7 The HNLC station (cluster 5)

At station R-2, dFe concentrations were low within surface waters (~ 0.1 nmol L^{-1}) and highest at 500 m depth (0.39 nmol L^{-1}) (Fig. 4e). Below 500 m, dFe concentrations decreased to a value of ~ 0.30 nmol L^{-1}.

The KEOPS, CROZEX and South Shetland Islands studies (Planquette et al., 2007; Blain et al., 2008; Nielsdóttir et al., 2012) presented comparable ranges of dFe at open ocean stations (Table 2). Dissolved Fe concentrations at R-2 were similar to those observed during KEOPS1 at C11 and the Kerfix station within the upper 170 m of the water column, but also between 700 and 1300 m (Blain et al., 2008). However, dFe concentrations were up to 6.5 fold higher between 200 and 500 m at R-2 compared to C-11 and Kerfix, despite the close proximity of Kerfix and R-2.

While sea-surface lithogenic silica (LSi) concentrations (Lasbleiz et al., 2014) were low at station R-2 (< 0.042 µmol L^{-1}), they were maximum at 500 m depth (0.12 µmol L^{-1}). Particulate Fe, manganese and aluminium (fraction between 1 µm and 55 µm) enrichments were also observed at 500 m (van der Merwe et al., 2015). These authors also observed a unique particulate trace metal composition signature at this station, which could originate from the Leclaire Rise, contrasting with the basaltic signature observed above the Kerguelen Plateau (Doucet et al., 2005). The Leclaire Rise is a remarkable oceanic feature that consists of a submerged volcano with an area of 6,500 km^2, with the shallowest depth up to 100 m. It is located 75 km north west of R-2 and could release dissolved and particulate material.

Similarly to clusters 3 and 4, remineralization may also partly explain dFe concentrations in the mesopelagic zone ($dFe = 0.0012 \pm 0.0002 \times AOU + 0.22 \pm 0.02$, n= 6, $r^2 = 91.8\%$, $p < 0.01$). Fe and C are also remineralized at the same rates as in clusters 3 and 4 (ANOVA, $p > 0.1$) and the intercept, significantly different from zero (ANOVA, $p < 0.01$), confirms the hypothesis of dFe sedimentary inputs at this station.

4 Conclusions

This third cruise over the Kerguelen Plateau allowed new insights into dFe sources and internal cycling. Direct runoff, glacial and sedimentary inputs can all be considered as important sources of dFe in the vicinity of Kerguelen Island. Remineralization of sinking particles can explain the high concentrations of dFe in intermediate waters offshore. The strong jet of the PF was enriched with dFe from the north of the plateau as it flowed northward close to Kerguelen Island and later eastward to loop back into the recirculation area. This fertilised surface waters of the eastern part of the studied area. Furthermore, filaments crossing the PF allowed a more direct natural Fe fertilisation of surface water in the recirculation area. Due to variable water mass origin and variable horizontal advection mechanism (along or across the PF), the recirculation area evidenced strong dFe concentration variability. The PF is an important Southern Ocean feature that should not be neglected with regards to Southern Ocean fertilisation offshore from the Kerguelen Plateau through fast lateral Fe transport from the north of the Kerguelen Plateau.

Acknowledgements

The authors thank the crew of the R/V Marion-Dufresne for assistance on board and Bernard Quéguiner, the chief scientist. They also greatly acknowledge Young-Hyang Park for fruitful discussions about the complex hydrography of the studied area. The authors thank two anonymous referees for their fruitful comments. This work was supported by the French Research program of INSU-CNRS LEFE−CYBER (‘Les enveloppes fluides et l'environnement’ – ‘Cycles biogéochimiques, environnement et ressources’), the French ANR (‘Agence Nationale de la Recherche’, SIMI-6 program, ANR-2010-BLAN-614 KEOPS2 and, ANR-10-JCJC-606 ICOP), the French CNES program (‘Centre National d’Etudes Spatiales’) and the French Polar Institute IPEV (Institut Polaire Paul−Emile Victor). This research was supported by University of Tasmania Cross Theme (B0018994) and Rising Stars (B0019024) grants. Thanks to the Antarctic Climate and Ecosystems Cooperative Research Centres (ACE CRC) for funding participation in the KEOPS2 study through the Carbon program. The KEOPS2 experiment was approved as a GEOTRACES process study.

References

Ardelan, M.V., Holm-Hansen, O., Hewes, C.D., Reiss, C.S., Silva, N.S., Dulaiova, H., Steinnes, E. and Sakshaug, E., 2010. Natural iron enrichment around the Antarctic Peninsula in the Southern Ocean. Biogeosciences, 7(1): 11-25.

Armand, L.K., Cornet-Barthaux, V., Mosseri, J. and Quéguiner, B., 2008. Late summer diatom biomass and community structure on and around the naturally iron-fertilised Kerguelen Plateau in the Southern Ocean. Deep Sea Res. II, 55: 653–676.

Berthier, E., Le Bris, R., Mabileau, L., Testut, L. and Rémy, F., 2009. Ice wastage on the Kerguelen Islands (49S, 69E) between 1963 and 2006. J. Geophys. Res. Earth Surface, 114: F03005, doi: 10.1029/2008JF001192.

Blain, S., Quéguiner, B., Armand, L., Belviso, S., Bombled, B., Bopp, L., Bowie, A., Brunet, C., Brussaard, C., Carlotti, F., Christaki, U., Corbière, A., Durand, I., Ebersbach, F., Fuda, J.-L., Garcia, N., Gerringa, L., Griffiths, B., Guigue, C., Guillerm, C., Jacquet, S., Jeandel, C., Laan, P., Lefèvre, D., Lomonaco, C., Malits, A., Mosseri, J., Obernosterer, I., Park, Y.-H., Picheral, M., Pondaven, P., Remenyi, T., Sandroni, V., Sarthou, G., Savoye, N., Scouarnec, L., Souhaut, M., Thuiller, D., Timmermans, K., Trull, T., Uitz, J., van-Beek, P., Veldhuis, M., Vincent, D., Viollier, E., Vong, L. and Wagener, T., 2007. Impact of natural iron fertilization on carbon sequestration in the Southern Ocean. Nature, 7139: 1070-1074.

Blain, S., Sarthou, G. and Laan, P., 2008. Distribution of DFe during the natural iron-fertilization experiment KEOPS. Deep Sea Res. II, 55: 594–605, doi:10.1016/j.dsr2.2007.12.028.

Bowie, A.R., Lannuzel, D., Remenyi, T.A., Wagener, T., Lam, P.J., Boyd, P.W., Guieu, C., Townsend, A.T. and Trull, T.W., 2009. Biogeochemical iron budgets of the Southern Ocean south of Australia: Decoupling of iron and nutrient cycles in the subantarctic zone by the summertime supply. Global Biogeochem. Cy., 23: GB4034, doi:10.1029/2009GB003500.

Bowie, A.R., van der Merwe, P., Quéroué, F., Trull, T., Fourquez, M., Planchon, F., Sarthou, G., Chever, F., Townsend, A.T., Obernosterer, I., Sallee, J.-B. and Blain, S., 2014. Iron budgets for three distinct biogeochemical sites around the Kerguelen archipelago (Southern Ocean) during the natural fertilisation experiment KEOPS-2. . Biogeosciences Discuss.

Bucciarelli, E., Blain, S. and Tréguer, P., 2001. Iron and manganese in the wake of the Kerguelen Islands (Southern Ocean). Mar. Chem., 73(1): 21-36.

Chase, Z., Johnson, K.S., Elrod, V.A., Plant, J.N., Fitzwater, S.E., Pickella, L. and Sakamotob, C.M., 2005. Manganese and iron distributions off central California influenced by upwelling and shelf width. Mar. Chem., 95: 235-254.

Chever, F., Sarthou, G., Bucciarelli, E., Blain, S. and Bowie, A.R., 2010. An iron budget during the natural iron fertilisation experiment KEOPS (Kerguelen Islands, Southern Ocean). Biogeosciences, 7: 455-468.

511 Closset, I., Lasbleiz, M., Leblanc, K., Quéguiner, B., Cavagna, A.-J., Elskens, M., Navez, J.
512 and Cardinal, D., 2014. Seasonal evolution of net and regenerated silica production
513 around a natural Fe-fertilized area in the Southern Ocean estimated with Si isotopic
514 approaches. Biogeosciences, 11: 5827-5846, doi:10.5194/bg-11-5827-2014.

515 Cutter, G., Andersson, P., Codispoti, L., Croot, P., Francois, R., Lohan, M., Obata, H. and
516 Rutgers van der Loeff, M., 2010. Sampling and Sample-handling Protocols for
517 GEOTRACES Cruises. Cookbook: hdl:10013/epic.42722.

518 Cutter, G.A., 2013. Intercalibration in chemical oceanography-Getting the right number.
519 Limnol. Oceanogr.: Methods, 11: 418-424.

520 d'Ovidio, F., Penna, A.D., Trull, T.W., Nencioli, F., Pujol, I., Rio, M.H., Park, Y.-H., Cotté,
521 C., Zhou, M. and Blain, S., 2014. The biogeochemical structuring role of horizontal
522 stirring: Lagrangian perspectives on iron delivery downstream of the Kerguelen
523 plateau. Biogeosciences Discuss., 12: 779-814, doi:10.5194/bgd-12-779-2015,
524 www.biogeosciences-discuss.net/12/779/2015/.

525 Doucet, S., Scoates, J.S., Weis, D. and Giret, A., 2005. Constraining the components of the
526 Kerguelen mantle plume: A Hf-Pb-Sr-Nd isotopic study of picrites and high-MgO
527 basalts from the Kerguelen Archipelago. Geochem. Geophys. Geosys., 6: Q04007,
528 doi: 10.1029/2004GC000806.

529 Dulaiova, H., Ardelan, M.V., Henderson, P.B. and Charette, M.A., 2009. Shelf-derived iron
530 inputs drive biological productivity in the southern Drake Passage. Global
531 Biogeochem. Cy., 23(4): DOI: 10.1029/2008GB003406.

532 Elrod, V.A., Berelson, W.M., Coale, K.H. and Johnson, K.S., 2004. The flux of iron from
533 continental shelf sediments: A missing source for global budgets. Geophys. Res. Lett.,
534 31, L12307: doi:10.1029/2004GL020216, 2004.

535 Frenot, Y., Van Vliet-Lanoë, B. and Gloaguen, J.-C., 1995. Particle translocation and initial
536 soil development n a Glacier Foreland, Kerguelen Islands, Subantarctic. Arctic Alpine
537 Res., 27(2): 107-115.

538 Gautier, I., Weis, D., Mennessier, J.-P., Vidal, P., Giret, A. and Loubet, M., 1990. Petrology
539 and geochemistry of the Kerguelen Archipelago basalts (South Indian Ocean)
540 evolution of the mantle sources from ridge to intraplate position. Earth Planet. Sci.
541 Lett., 100: 59-76.

542 Hatta, M., Measures, C.I., Selph, K.E., Zhou, M. and Hiscock, W.T., 2013. Iron fluxes from
543 the shelf regions near the South Shetland Islands in the Drake Passage during the
544 austral-winter 2006. Deep Sea Res. II, 90: 89-101.

545 Hatta, M., Measures, C.I., Wu, J., Roshan, S., Fitzsimmons, J.N., Sedwick, P. and Morton, P.,
546 2014. An overview of dissolved Fe and Mn Distributions during the 2010–2011 U.S.
547 GEOTRACES north Atlantic Cruises: GEOTRACES GA03. Deep-Sea Res. II, in
548 press: http://dx.doi.org/10.1016/j. dsr2.2014.07.005.

549 Heimburger, A., Losno, R., Triquet, S. and Nguyen, E.B., 2013. Atmospheric deposition
550 fluxes of 26 elements over the Southern Indian Ocean: time series on Kerguelen and
551 Crozet Islands. Global Biogeochem. Cy., 27(2): 440–449, DOI: 10.1002/gbc.20043.

552 Homoky, W.B., John, S.G., Conway, T.M. and Mills, R.A., 2013. Distinct iron isotopic
553 signatures and supply from marine sediment dissolution. Nature communications,
554 4(Article number: 2143): DOI: 10.1038/ncomms3143.

555 Ibisanmi, E., Sander, S.G., Boyd, P.W., Bowie, A.R. and Hunter, K.A., 2011. Vertical
556 distributions of iron-(III) complexing ligands in the Southern Ocean. Deep Sea
557 Research Part II: Topical Studies in Oceanography, 58(21–22): 2113-2125.

558 Jickells, T.D., An, Z.S., Andersen, K.K., Baker, A.R., Bergametti, G., Brooks, N., Cao, J.J.,
559 Boyd, P.W., Duce, R.A., Hunter, K.A., Kawahata, H., Kubilay, N., La Roche, J., Liss,
560 P.S., Mahowald, N., Prospero, J.M., Ridgwell, A.J., Tegen, I. and Torres, R., 2005.
561 Global Iron Connections Between Desert Dust, Ocean Biogeochemistry, and Climate.
562 Science, 308: 67-71.

563 Johnson, K.S., Chavez, F.P. and Friederich, G.E., 1999. Continental shelf sediments as a
564 primary source of iron to coastal phytoplankton. Nature, 398: 697-700.

565 Johnson, K.S., Boyle, E., Bruland, K., Coale, K., Measures, C., Moffett, J., Aguilar-Islas, A.,
566 Barbeau, K., Bergquist, B., Bowie, A., Buck, K., Cai, Y., Chase, Z., Cullen, J., Doi,
567 T., Elrod, V., Fitzwater, S., Gordon, M., King, A., Laan, P., Laglera-Baquer, L.,
568 Landing, W., Lohan, M., Mendez, J., Milne, A., Obata, H., Ossiander, L., Plant, J.,
569 Sarthou, G., Sedwick, P., Smith, G., Sohst, B., Tanner, S., Van den Berg, C.M.G. and
570 Wu, J., 2007. Developping standards for dissolved iron in seawater. EOS
571 Transactions, American Geophysical Union, 88(11): 131–132.

572 Klunder, M.B., Laan, P., De Baar, H.J.W., Middag, R., Neven, I. and Van Ooijen, J., 2014.
573 Dissolved Fe across the Weddell Sea and Drake Passage: impact of DFe on nutrient
574 uptake. Biogeosciences, 11: 651–669, doi:10.5194/bg-11-651-2014,
575 www.biogeosciences.net/11/651/2014/.

576 Lam, P.J., Bishop, J.K.B., Henning, C.C., Marcus, M.A., Waychunas, G.A. and Fung, I.Y.,
577 2006. Wintertime phytoplankton bloom in the subarctic Pacific supported by
578 continental margin iron. Global Biogeochem. Cy., 20(GB1006):
579 doi:10.1029/2005GB002557.

580 Lam, P.J. and Bishop, J.K.B., 2008. The continental margin is a key source of iron to the
581 HNLC North Pacific Ocean. Geophys. Res. Lett., 35 L07608,
582 doi:10.1029/2008GL033294.

583 Lasbleiz, M., Leblanc, K., Blain, S., Ras, J., Cornet-Barthaux, V., Nunige, S.H. and
584 Quéguiner, B., 2014. Pigments, elemental composition (C, N, P, Si) and stoichiometry
585 of particulate matter, in the naturally iron fertilized region of Kerguelen in the
586 Southern Ocean. Biogeosciences, 11: 5931–5955, doi:10.5194/bg-11-5931-2014,
587 www.biogeosciences.net/11/5931/2014/

588 Marsay, C.M., Sedwick, P.N., Dinninman, M.S., Barrett, P.M., Mack, S.L. and McGillicuddy
589 Jr, D.J., 2014. Estimating the benthic efflux of dissolved iron on the Ross Sea
590 continental shelf. Geophys. Res. Lett., 41(21): 7576-7583, DOI:
591 10.1002/2014GL061684.

592 Martin, J.H., Knauer, G.A., Karl, D.M. and Broenkow, W.W., 1987. VERTEX: carbon
593 cycling in the northeast Pacific. Deep-Sea Res. I, 34: 267-285.

Measures, C.I., Brown, M.T., Selph, K.E., Apprill, A., Zhou, M., Hatta, M. and Hiscock, W.T., 2013. The influence of shelf processes in delivering dissolved iron to the HNLC waters of the Drake Passage, Antarctica. Deep Sea Research Part II: Topical Studies in Oceanography, 90: 77-88.

Moore, J.K., Doney, S.C., Glover, D.M. and Fung, I.Y., 2001. Iron cycling and nutrient limitation patterns in surface waters of the World Ocean. Deep Sea Res. II, 49(1-3): 463-507.

Morris, P.J. and Charette, M.A., 2013. A synthesis of upper ocean carbon and dissolved iron budgets for Southern Ocean natural iron fertilisation studies. Deep Sea Res. II, 90: 147-157.

Nielsdóttir, M.C., Bibby, T.S., Moore, C.M., Hinz, D.J., Sanders, R., Whitehouse, M., Korb, R. and Achterberg, E.P., 2012. Seasonal and spatial dynamics of iron availability in the Scotia Sea. Mar. Chem., 130–131: 62-72.

Obata, H., Karatani, H. and Nakayama, E., 1993. Automated determination of iron in seawater by chelating resin concentration and chemiluminescence. Anal. Chem., 65: 1524-1528.

Park, Y.-H., Durand, I., Kestenare, E., Rougier, G., Zhou, M., d'Ovidio, F., Cotté, C. and Lee, J.-H., 2014. Polar Front around the Kerguelen Islands: An up-to-date determination and associated circulation of surface/subsurface waters. J. Geophys. Res. Oceans, 119(10): 6575-6592, doi:10.1002/2014JC010061.

Planquette, H., Sanders, R.R., Statham, P.J., Morris, P.J. and Fones, G.R., 2011. Fluxes of particulate iron from the upper ocean around the Crozet Islands: A naturally iron-fertilized environment in the Southern Ocean. Global Biogeochem. Cycles, 25: GB2011-GB2011.

Planquette, H.F., Statham, P.J., Fones, G.R., Charette, M.A., Moore, C.M., Salter, I., Nédélec, F.H., Taylor, S.L., French, M., Baker, A.R., Mahowald, N. and Jickells, T.D., 2007. Dissolved iron in the vicinity of the Crozet Islands, Southern Ocean. Deep-Sea Res. II, 54(18-20, [doi:10.1016/j.dsr2.2007.07.019]): 1999–2019.

Pollard, R.T., Salter, I., Sanders, R.J., Lucas, M.I., Moore, C.M., Mills, R.A., Statham, P.J., Allen, J.T., Baker, A.R., Bakker, D.C.E., Charette, M.A., Fielding, S., Fones, G.R., French, M., Hickman, A.E., Holland, R.J., Hughes, J.A., Jickells, T.D., Lampitt, R.S., Morris, P.J., Nédélec, F.H., Nielsdottir, M., Planquette, H., Popova, E.E., Poulton, A.J., Read, J.F., Seeyave, S., Smith, T., Stinchcombe, M., Taylor, S., Thomalla, S., Venables, H.J., Williamson, R. and Zubkov, M.V., 2009. Southern Ocean deep-water carbon export enhanced by natural iron fertilization. Nature, 457: 577-580, doi:10.1038/nature07716.

Raiswell, R., Vu, H.P., Brinza, L. and Benning, L.G., 2010. The determination of labile Fe in ferrihydrite by ascorbic acid extraction: methodology, dissolution kinetics and loss of solubility with age and de-watering. Chem. Geol., 278: 70-79.

Raiswell, R., 2011. Iceberg-hosted nanoparticulate Fe in the Southern Ocean: Mineralogy, origin, dissolution kinetics and source of bioavailable Fe. Deep Sea Res. II, 58(11-12): 1364-1375, http://dx.doi.org/10.1016/j.dsr2.2010.11.011.

636 Sanial, V., van Beek, P., Lansard, B., Souhaut, M., Kestenare, E., d'Ovidio, F., Zhou, M. and
637 Blain, S., 2015. Use of Ra isotopes to deduce rapid transfer of sediment-derived inputs
638 off Kerguelen. Biogeosciences, 12: 1415–1430, doi:10.5194/bg-12-1415-2015,
639 www.biogeosciences.net/12/1415/2015/.

640 Sarthou, G., Baker, A.R., Blain, S., Achterberg, E.P., Boye, M., Bowie, A.R., Croot, P.L.,
641 Laan, P., de Baar, H.J.W., Jickells, T.D. and Worsfold, P.J., 2003. Atmospheric iron
642 deposition and sea-surface dissolved iron concentrations in the eastern Atlantic Ocean.
643 Deep Sea Res. I, 50(10-11): 1339-1352.

644 Sarthou, G., Timmermans, K.R., Blain, S. and Tréguer, P., 2005. Growth physiology and fate
645 of diatoms in the ocean: a review. J. Sea Res., 53(1-2): 25-42.

646 Savoye, N., Trull, T.W., Jacquet, S.H.M., Navez, J. and Dehairs, F., 2008. ^{234}Th-based export
647 fluxes during a natural iron fertilization experiment in the Southern Ocean (KEOPS).
648 Deep Sea Res. II, 55: 841–855.

649 Smith Jr, W.O., Sedwick, P.N., Arrigo, K.R., Ainley, D.G. and Orsi, A.H., 2012. The Ross
650 Sea in a sea of change. Oceanography, 25: 44-57.

651 Sunda, W.G. and Huntsman, S.A., 1995. Iron uptake and growth limitation in oceanic and
652 coastal phytoplankton. Mar. Chem., 50(1-4): 189-206.

653 Sunda, W.G., 1997. Control of dissolved iron concentrations in the world ocean: A comment.
654 Mar. Chem., 57: 169-172.

655 Tagliabue, A., Bowie, A., Chever, F., Baptiste, P.-J., Dutay, J.-C., Bucciarelli, E., Lannuzel,
656 D., Remenyi, T., Sarthou, G., Aumont, O., Gehlen, M. and Bopp, L., 2010. On the
657 importance of hydrothermalism to the oceanic dissolved iron inventory. Nature
658 Geoscience, 3: 252-256, DOI: 10.1038/NGEO818.

659 Tagliabue, A., Mtshali, T., Aumont, O., Bowie, A.R., Klunder, M.B., Roychoudhury, A.N.
660 and Swart, S., 2012. A global compilation of dissolved iron measurements: focus on
661 distributions and processes in the Southern Ocean. Biogeosciences, 9: 2333–2349,
662 2012, www.biogeosciences.net/9/2333/2012/, doi:10.5194/bg-9-2333-2012.

663 Thuróczy, C.-E., Gerringa, L.J.A., Klunder, M.B., Laan, P. and de Baar, H.J.W., 2011.
664 Observation of consistent trends in the organic complexation of dissolved iron in the
665 Atlantic Sector of the Southern Ocean. Deep Sea Res. II, 58: 2695–2706.

666 Twining, B.S., Baines, S.B. and Fisher, N.S., 2004. Element stoichiometries of individual
667 plankton cells collected during the Southern Ocean Iron Experiment (SOFeX).
668 Limnol. Oceanogr., 49(6): 2115-2128.

669 van der Merwe, P., Bowie, A.R., Quéroué, F., Armand, L., Blain, S., Chever, F., Davies, D.,
670 Dehairs, F., Planchon, F., Sarthou, G., Townsend, A.T. and Trull, T., 2015. Sourcing
671 the iron in the naturally-fertilised bloom around the Kerguelen Plateau: particulate
672 trace metal dynamics Biogeosciences, 12: 1-17, doi:10.5194/bg-12-739-2015.

673 Wagener, T., Guieu, C., Losno, R., Bonnet, S. and Mahowald, N., 2008. Revisiting
674 atmospheric dust export to the Southern Hemisphere ocean: Biogeochemical
675 implications. Global Biogeochem. Cycles, 22: GB2006, doi:10.1029/2007GB002984.

676 Walsh, I., Fischer, K., Murray, D. and Dymond, J., 1988. Evidence for resuspension of
677 rebound particles from near-bottom sediment traps. Deep-Sea Res. I, 35: 59-70.

678

679
680

Figure captions

Figure 1: Map showing the bathymetry of the area and the stations visited during KEOPS2 (yellow-orange for cluster 1, green for Cluster 2, blue-violet for cluster 3, brown for cluster 4, and grey for cluster 5), KEOPS1 (blue dots; Blain et al., 2008), and ANTARES3 (black dots; Bucciarelli et al., 2001). The dashed line represents the approximate location of the polar front (200 m) (Park et al., 2014).

Figure 2: Temperature-Salinity diagram for stations sampled during KEOPS2 for dissolved iron. Water masses are indicated in black, and station names in grey. The same colour code as used in Figure 1 applies here.
(A) Clusters 1 and 2: near-coastal (TEW-1, TEW-2) and Kerguelen Plateau (A3-1, A3-2, G-1, TEW-3) stations. Three water masses are displayed: surface water (SW), winter water (WW), upper circumpolar deep water (UCDW). (B) Cluster 3: the recirculation area (E-2, TEW-4, TEW-5, E-3, E-4W-2, E-5). Four water masses are displayed: surface water (SW), winter water (WW), upper circumpolar deep water (UCDW), lower circumpolar deep water (LCDW). (C) Clusters 4 and 5: north of the polar front (F-L, TEW-7) and the HNLC area (R2). Five water masses are displayed: sub-antarctic surface water (SASW), antarctic intermediate water (AAIW), winter water (WW), upper circumpolar deep water (UCDW), lower circumpolar deep water (LCDW).

Figure 3: A boxplot of the dFe concentrations in each water mass present in clusters 2 to 5: Surface waters (SW and SASW), winter waters (WW), Antarctic intermediate water (AAIW), and lower and upper circumpolar deep water (LCDW and UCDW). Median values are indicated by a horizontal line within the box, the box represents the interquartile range, and the whiskers extend to 5^{th} and 95^{th} percentile values. Data from cluster 1 are not shown to allow a clearer representation of the other clusters.

Figure 4: Vertical distribution of dFe concentrations measured in clusters 1 (a), 2 (b), 3 (c), 4 (d) and 5 (e) showing the median dFe (solid line with crosses). The interquartile range defined

711 as the range around the median containing 50% of the data is given between the two dotted
712 lines.

713

714 Figure 5: Concentrations of dFe (nmol L^{-1}) over the East-West transect. The PF position is
715 indicated with black dashed lines. Stations TEW-1, TEW-2, TEW-3, TEW-4, E-2, TEW-5,
716 TEW-7 and F-L were included in this section as they were sampled consecutively in a short
717 time period (7 days) (Table 1).

718

719 Figure 6. (a) Dissolved Fe concentrations, (b) beam attenuation coefficient, and (c) total
720 chlorophyll-a concentrations (from Lasbleiz et al., 2014) at near-coastal stations (cluster 1,
721 TEW-1 and TEW-2), stations above the Plateau (cluster 2, A3-1, A3-2, G-1 and TEW-3) and
722 at E-4W-2. The same colour code as used in Figure 1 applies here.

723

724 Figure 7: Dissolved Fe concentrations as a function of height above seafloor for all the
725 stations of cluster 2. Bottom depths are taken from the CTD data. The same colour code as
726 used in Figure 1 applies here.

727 Figure 8: dFe vs. AOU in the recirculation area at stations E-2, E-5, TEW-4, TEW-5, E-4W-
728 2, E-3, R-2, and TEW-7 and F-L. The deeper dFe concentration at station E-4W-2 was not
729 included since the observed sedimentary inputs would have masked the remineralization
730 signal. The same colour code as used in Figure 1 applies here.

Table 1. Station name, longitude, latitude, sampling date, mixed layer depth (MLD), station bottom depth, location, dissolved iron concentrations (dFe) and standard deviation (STD) during KEOPS2. MLD were estimated using, as a reference, potential densities at both 10 m and 20 m. When estimates are different, both values are given.

Station	Long [degree-east]	Lat [degree-south]	Date	MLD [m]	Bot depth [m]	Depth [m]	dFe [nmol L^{-1}]	STD [nmol L^{-1}]
A3-1	72.06	50.62	20/10/11	164-165	530	45	0.28	0.00
						105	0.40	0.01
						160	0.32	0.02
						340	0.53	0.03
R2	66.68	50.38	26/10/11	76-95	2500	40	0.09	0.01
						70	0.08	0.01
						100	0.17	0.00
						140	0.18	0.01
						170	0.12	0.01
						200	0.27	0.00
						235	0.26	0.00
						300	0.33	0.01
						350	0.35	0.01
						400	0.38	0.01
						500	0.39	0.01
						700	0.28	0.02
						900	0.28	0.01
						1000	0.31	0.02
						1200	0.30	0.01
						1300	0.32	0.01
TEW-1	69.83	49.13	31/10/11	32-42	86	15	1.82	0.38
						40	2.52	0.12
						50	2.58	0.16
						62	3.82	0.04
TEW-2	70.65	48.88	31/10/11	40-70	85	15	1.26	0.03
						30	1.61	0.02
						40	1.70	0.14
						50	1.80	0.07
						62	1.82	0.01
TEW-3	71.02	48.78	31/10/11	16-94	560	20	0.19	0.02
						40	0.12	0.02
						70	0.09	0.01
						100	0.21	0.00

Station	Long [degree east]	Lat [degree south]	Date	MLD [m]	Bot depth [m]	Depth [m]	dFe [nmol L^{-1}]	STD [nmol L^{-1}]
						150	0.19	0.01
						200	0.19	0.01
						300	0.26	0.01
						400	0.37	0.00
						480	0.52	0.01
TEW-4	71.62	48.62	1/11/11	95	1600	40	0.17	0.02
						70	0.15	0.01
						100	0.20	0.01
						150	0.10	0.01
						200	0.11	0.00
						300	0.21	0.00
						400	0.30	0.00
						500	0.36	0.01
						600	0.39	0.01
						700	0.35	0.01
						1000	0.40	0.00
						1300	0.42	0.01
E-2	72.07	48.52	1/11/11	42-43	2000	40	0.08	0.01
						70	0.08	0.00
						100	0.10	0.00
						150	0.07	0.01
						200	0.18	0.00
						300	0.22	0.01
						400	0.23	0.01
						500	0.28	0.01
						600	0.34	0.01
						700	0.28	0.01
						1000	0.37	0.01
						1300	0.37	0.01
TEW-5	72.78	48.47	1/11/11	22-56	2250	40	0.12	0.01
						70	0.13	0.01
						100	0.16	0.01
						150	0.16	0.02
						200	0.21	0.08
						300	0.30	0.01
						400	0.39	0.01
						500	0.36	0.01
						600	0.31	0.01

Station	Long [degree east]	Lat [degree south]	Date	MLD [m]	Bot depth [m]	Depth [m]	dFe [nmol L^{-1}]	STD [nmol L^{-1}]
						700	0.34	0.01
						1000	0.44	0.01
						1300	0.42	0.01
TEW-7	73.98	48.45	2/11/11	22-24	2500	20	0.39	0.02
						40	0.22	0.02
						150	0.40	0.04
						200	0.46	0.02
						300	0.46	0.02
						400	0.48	0.02
						1000	0.56	0.01
						1300	0.59	0.02
E-3	71.97	48.70	3/11/11	32-35	1900	20	0.38	0.03
						40	0.31	0.02
						70	0.22	0.01
						100	0.24	0.01
						130	0.24	0.02
						200	0.33	0.01
						300	0.50	0.01
						400	0.46	0.01
						600	0.50	0.02
						800	0.50	0.02
						1000	0.50	0.01
						1300	0.52	0.01
F-L	74.65	48.52	7/11/11	47	2700	20	0.26	0.02
						35	0.17	0.03
						60	0.30	0.00
						100	0.33	0.01
						200	0.48	0.03
						300	0.40	0.03
						400	0.40	0.01
						600	0.56	0.03
						800	0.61	0.02
						1000	0.67	0.03
						1300	0.61	0.05
A3-2	72.05	50.62	16/11/11	123	525	37	0.18	0.02
						70	0.14	0.01
						108	0.14	0.01
						210	0.51	0.01

Station	Long [degree east]	Lat [degree south]	Date	MLD [m]	Bot depth [m]	Depth [m]	dFe [nmol L^{-1}]	STD [nmol L^{-1}]
						300	0.66	0.01
						400	0.81	0.02
						450	1.04	0.00
						480	1.30	0.01
G-1	71.88	49.90	9/11/11	60-68	590	20	0.21	0.04
						40	0.13	0.01
						70	0.23	0.01
						100	0.17	0.01
						150	0.19	0.01
						200	0.18	0.01
						250	0.24	0.01
						300	0.49	0.01
						350	0.67	0.01
						400	0.74	0.02
						500	0.59	0.02
						540	0.99	0.01
E-4W-2	71.42	48.75	18/11/11	26-35	1390	20	0.20	0.01
						40	0.16	0.01
						70	0.15	0.01
						100	0.11	0.00
						150	0.22	0.01
						180	0.28	0.00
						230	0.28	0.01
						300	0.35	0.01
						500	0.41	0.01
						700	0.42	0.01
						900	0.40	0.00
						1100	0.61	0.02
E-5	71.88	48.40	19/11/11	35-41	1920	25	0.06	0.01
						40	0.06	0.00
						70	0.10	0.00
						110	0.08	0.01
						150	0.11	0.01
						200	0.14	0.01
						350	0.23	0.00
						500	0.43	0.01
						700	0.37	0.00
						900	0.34	0.01

Station	Long [degree east]	Lat [degree south]	Date	MLD [m]	Bot depth [m]	Depth [m]	dFe [nmol L^{-1}]	STD [nmol L^{-1}]
						1100	0.40	0.00
						1300	0.39	0.03

Table 2. Concentrations of dissolved iron (nmol L^{-1}) for various Southern Ocean regions influenced by natural iron fertilisation. Near-coastal and shelf water stations were defined as stations where the bottom depth was less than 100 m and between 100m and 500 m depth, respectively. Furthermore near-coastal stations were less than 25 km distant from shore. The recirculation area corresponds to the polar front meander at the North-East of the Kerguelen Islands.

Location	Near-coastal	Shelf water	Recirculation	North polar front	HNLC	Sampling period	Reference
Kerguelen	1.26-3.82	0.09-1.30		0.17-0.67	0.08-0.39	spring	This Study
	0.78-0.81	0.05-0.71	0.08-0.17	-	0.05-0.38	summer	Blain et al., 2008
	5.04-22.60	0.26-1.74	0.46-2.71	0.88-4.11	-	spring	Bucciarelli et al., 2001
Crozet	0.39-2.16	0.15-0.42	-	0.22-0.38	0.20-0.40	late spring	Planquette et al., 2007
South Georgia	-	0.065-1.321	-	-	-	summer	Nielsdóttir et al., 2012
South Orkney	0.966-2.275	-	-	-	-	summer	Nielsdóttir et al., 2012
South Shetland	> 3	1.2-2.6	-	-	-	winter	Hatta et al., 2013
	0.8-2.2	-	-	-	-	late summer	Klunder et al., 2014

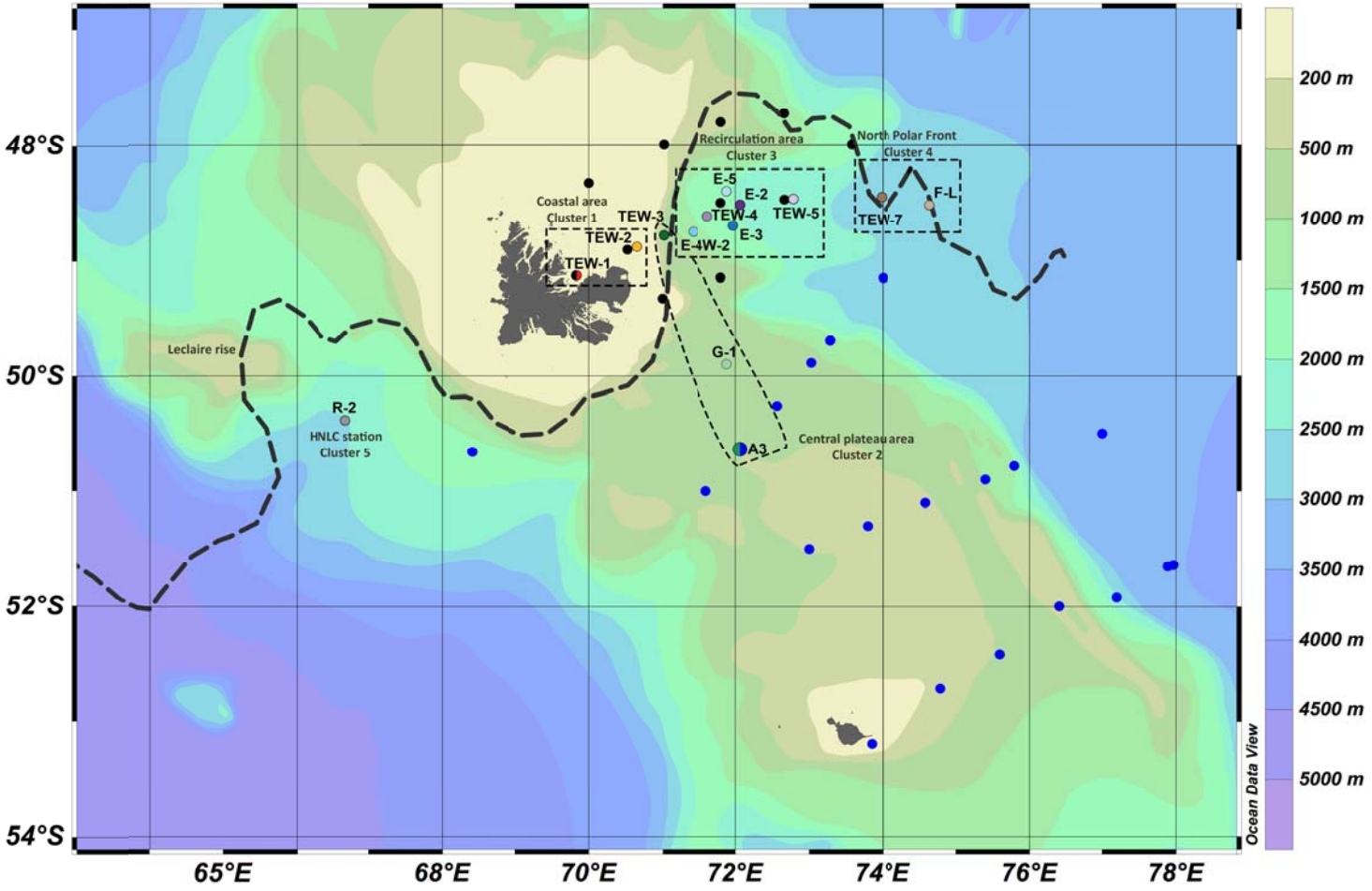
48°S
50°S
52°S
54°S
65°E
68°E
70°E
72°E
74°E
76°E
78°E
Recirculation area
Cluster 3
North Polar Front
Cluster 4
Coastal area
Cluster 1
Central plateau area
Cluster 2
HNLC station
Cluster 5
Leclaire rise
E-5
E-2
TEW-5
TEW-4
TEW-3
TEW-2
TEW-1
E-3
E-4W-2
F-L
TEW-7
G-1
R-2
A3
200 m
500 m
1000 m
1500 m
2000 m
2500 m
3000 m
3500 m
4000 m
4500 m
5000 m
Ocean Data View

Figure 1

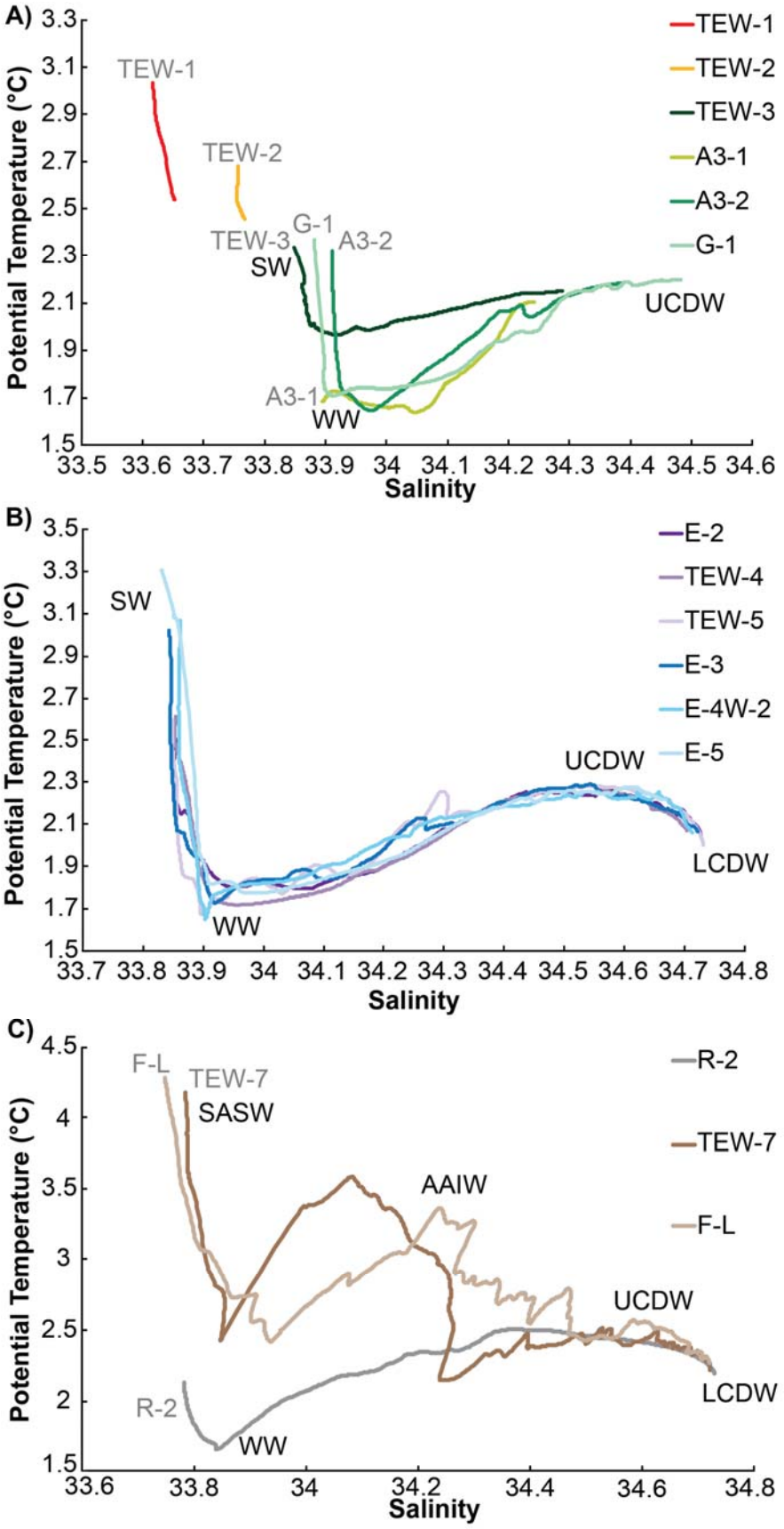
A)
Potential Temperature (°C)
Salinity
TEW-1
TEW-2
TEW-3
A3-1
A3-2
G-1
SW
UCDW
WW
B)
E-2
TEW-4
TEW-5
E-3
E-4W-2
E-5
LCDW
C)
F-L
TEW-7
SASW
AAIW
R-2

Figure 2

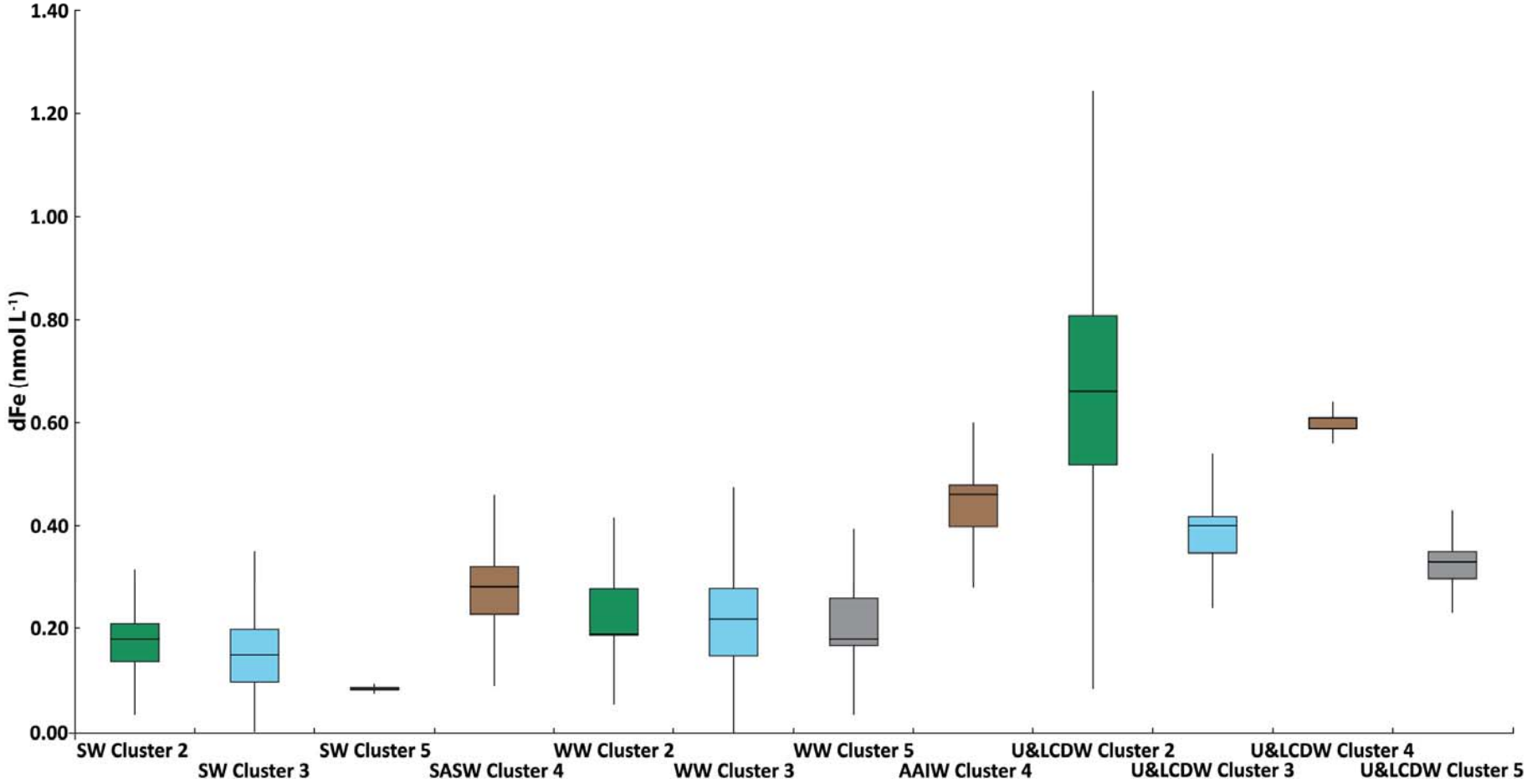
1.40
1.20
1.00
0.80
0.60
0.40
0.20
0.00
dFe (nmol L-1)
SW Cluster 2
SW Cluster 3
SW Cluster 5
SASW Cluster 4
WW Cluster 2
WW Cluster 3
WW Cluster 5
AAIW Cluster 4
U&LCDW Cluster 2
U&LCDW Cluster 3
U&LCDW Cluster 4
U&LCDW Cluster 5

Figure 3

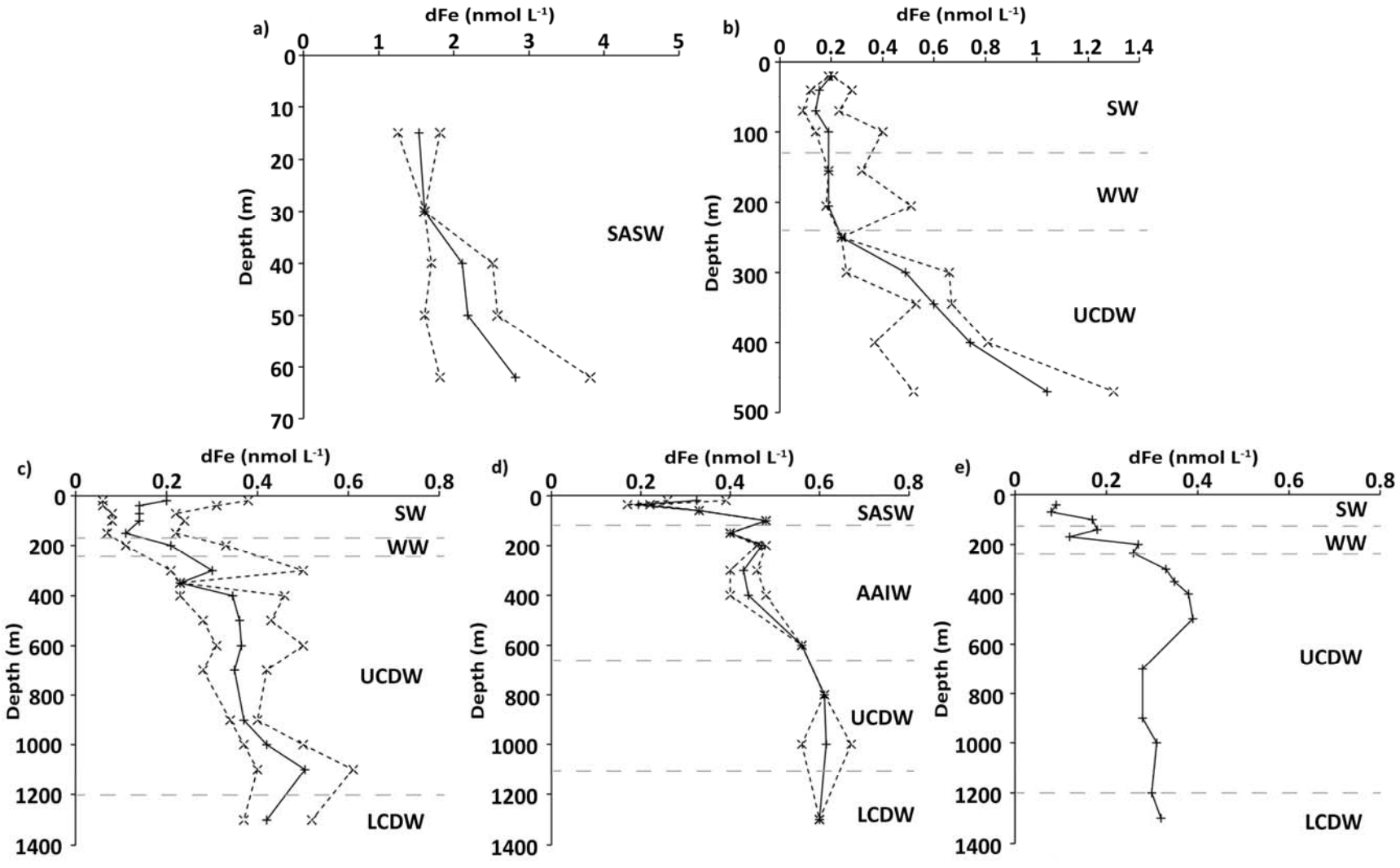
a)
dFe (nmol L-1)
0 1 2 3 4 5
Depth (m)
0 10 20 30 40 50 60 70
SASW
b)
dFe (nmol L-1)
0 0.2 0.4 0.6 0.8 1 1.2 1.4
Depth (m)
0 100 200 300 400 500
SW
WW
UCDW
c)
dFe (nmol L-1)
0 0.2 0.4 0.6 0.8
Depth (m)
0 200 400 600 800 1000 1200 1400
SW
WW
UCDW
LCDW
d)
dFe (nmol L-1)
0 0.2 0.4 0.6 0.8
Depth (m)
0 200 400 600 800 1000 1200 1400
SASW
AAIW
UCDW
LCDW
e)
dFe (nmol L-1)
0 0.2 0.4 0.6 0.8
Depth (m)
0 200 400 600 800 1000 1200 1400
SW
WW
UCDW
LCDW

Figure 4

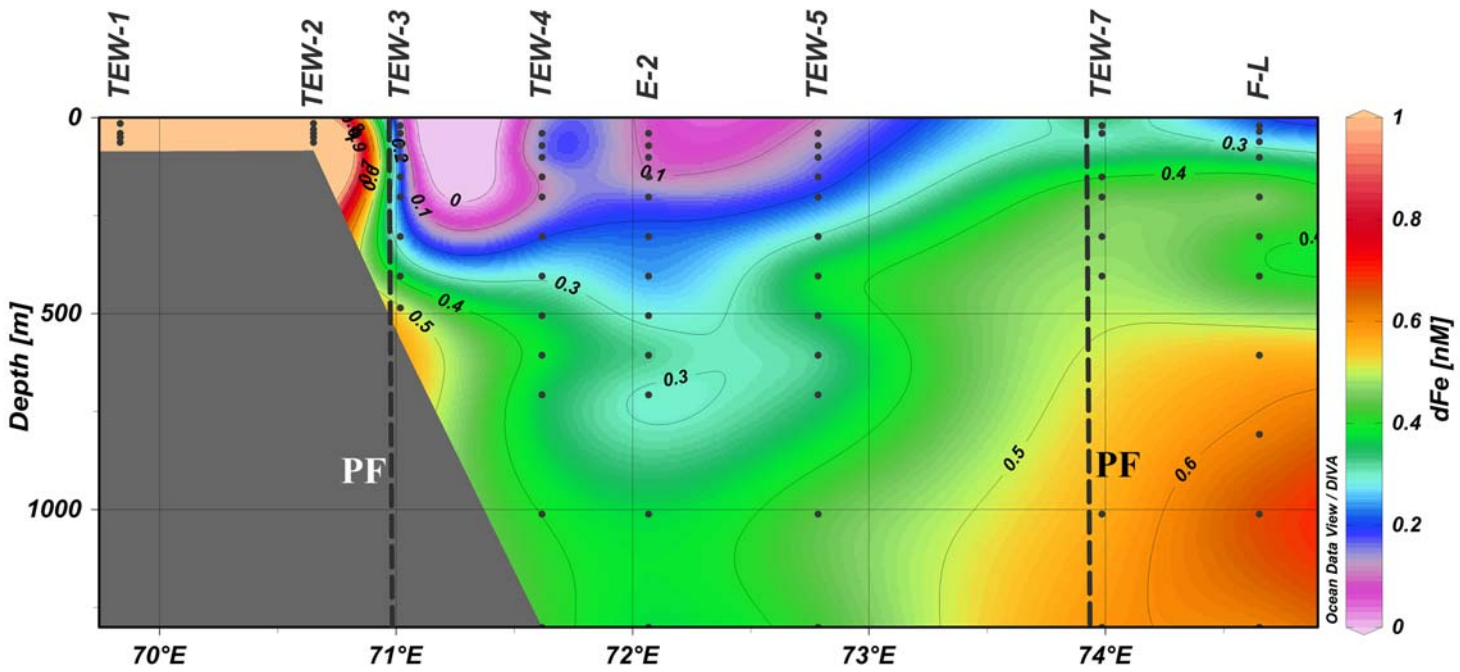
TEW-1
TEW-2
TEW-3
TEW-4
E-2
TEW-5
TEW-7
F-L
0
500
1000
Depth [m]
PF
PF
70°E
71°E
72°E
73°E
74°E
0.8
0.1
0
0.1
0.3
0.4
0.5
0.3
0.1
0.3
0.4
0.5
0.6
1
0.8
0.6
0.4
0.2
0
dFe [nM]
Ocean Data View / DIVA

Figure 5

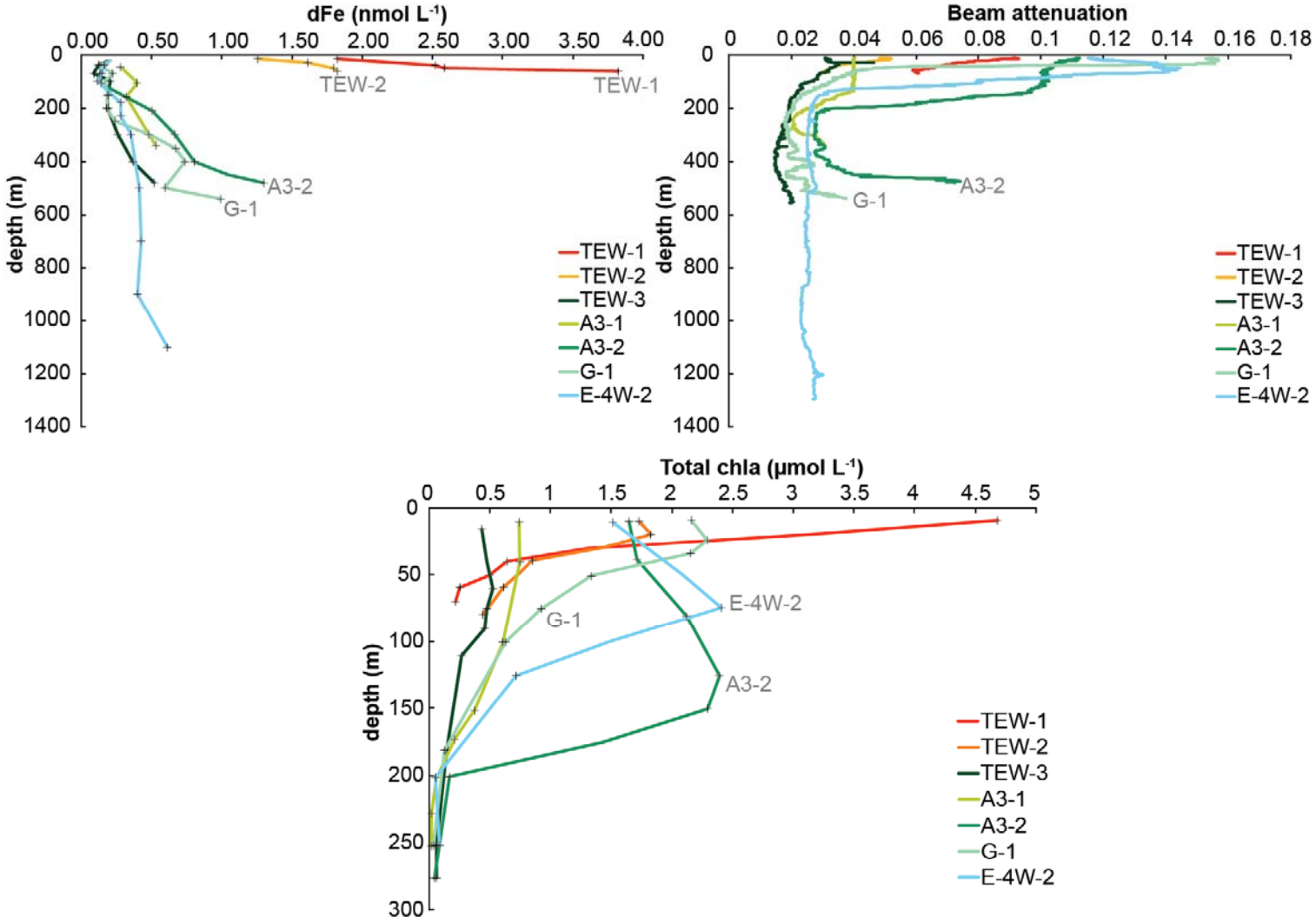
dFe (nmol L-1)
0.00 0.50 1.00 1.50 2.00 2.50 3.00 3.50 4.00
depth (m)
0 200 400 600 800 1000 1200 1400
TEW-2
TEW-1
A3-2
G-1
TEW-1
TEW-2
TEW-3
A3-1
A3-2
G-1
E-4W-2
Beam attenuation
0 0.02 0.04 0.06 0.08 0.1 0.12 0.14 0.16 0.18
depth (m)
0 200 400 600 800 1000 1200 1400
A3-2
G-1
TEW-1
TEW-2
TEW-3
A3-1
A3-2
G-1
E-4W-2
Total chla (µmol L-1)
0 0.5 1 1.5 2 2.5 3 3.5 4 4.5 5
depth (m)
0 50 100 150 200 250 300
E-4W-2
G-1
A3-2
TEW-1
TEW-2
TEW-3
A3-1
A3-2
G-1
E-4W-2

Figure 6

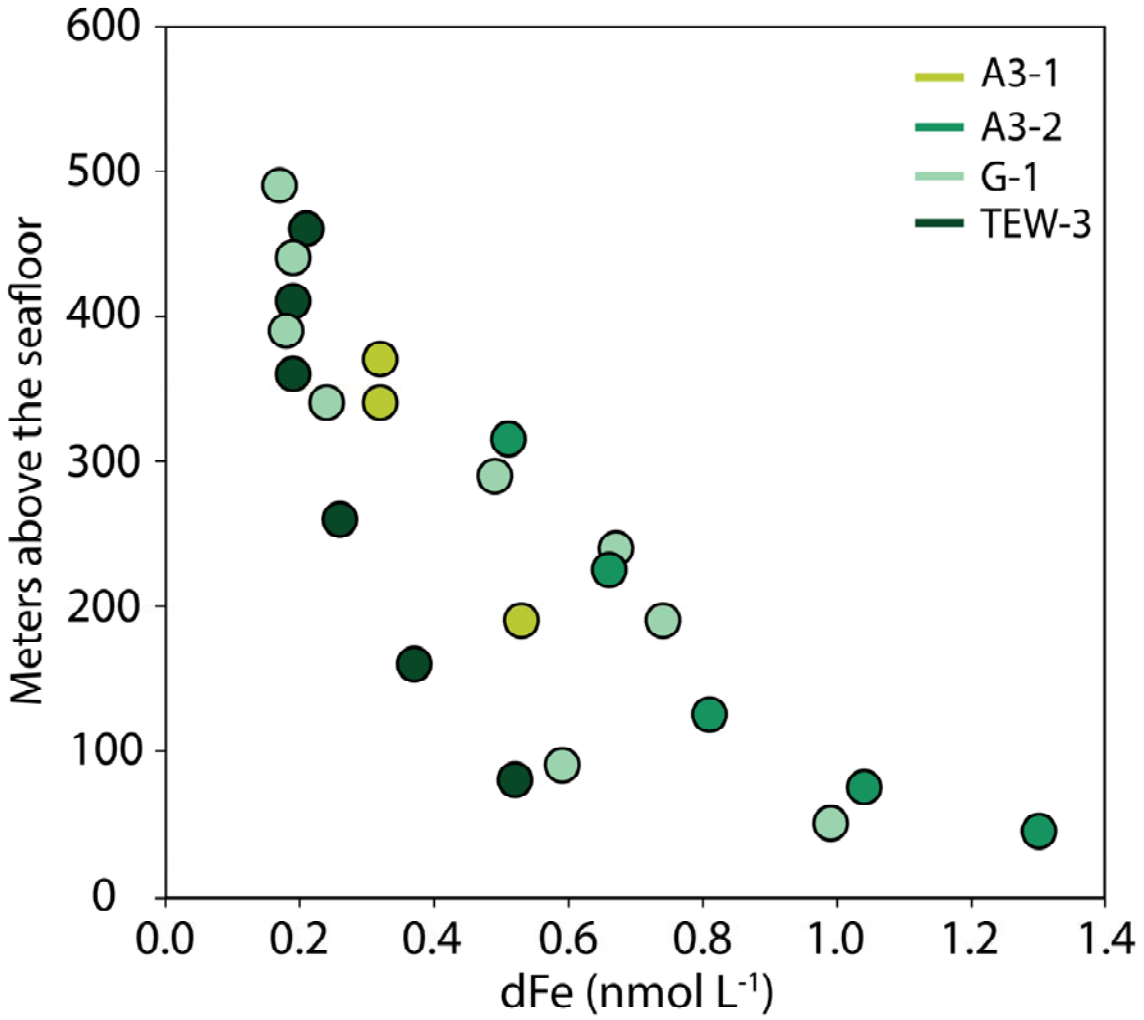
600
500
400
300
200
100
0
Meters above the seafloor
0.0
0.2
0.4
0.6
0.8
1.0
1.2
1.4
dFe (nmol L-1)
A3-1
A3-2
G-1
TEW-3

Figure 7

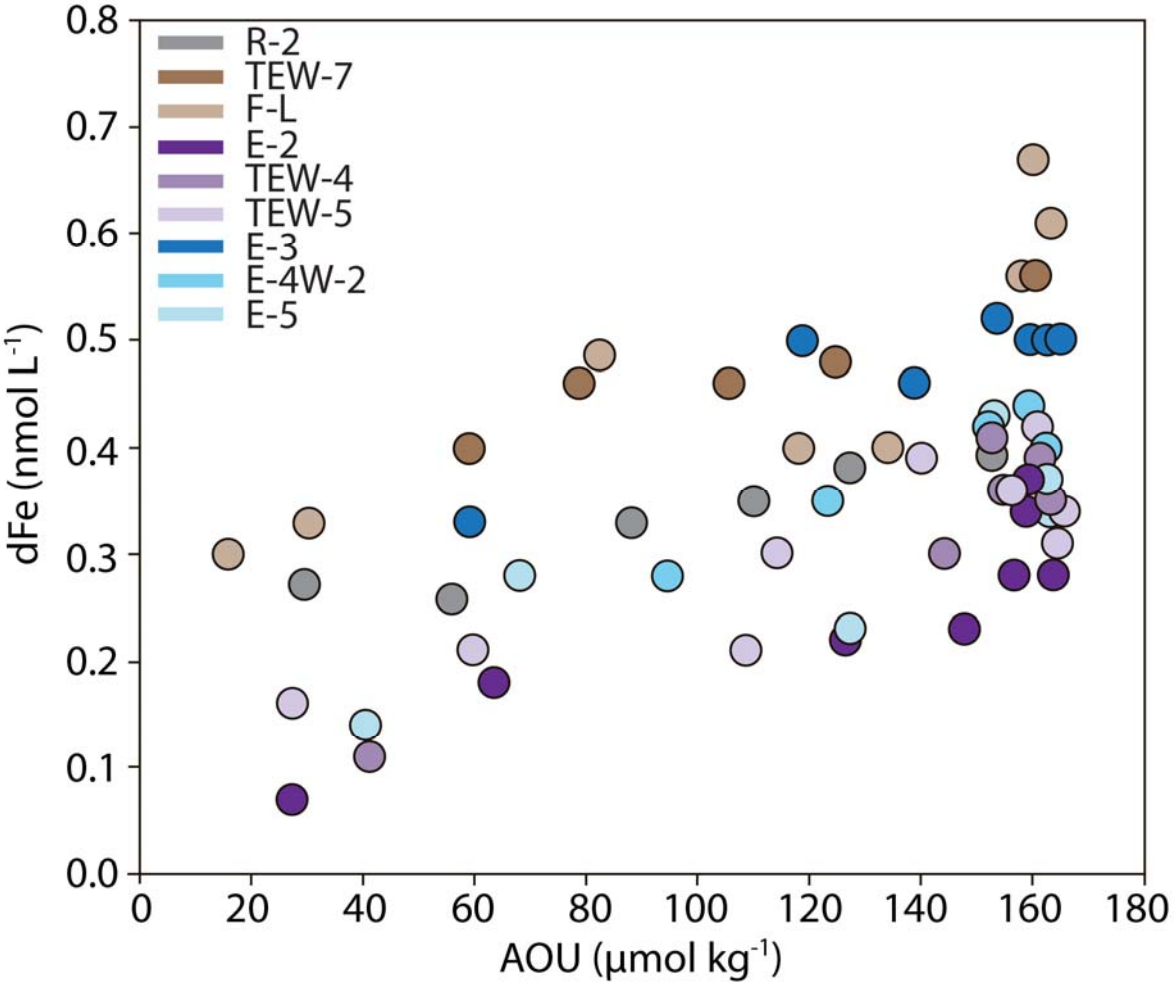
R-2
TEW-7
F-L
E-2
TEW-4
TEW-5
E-3
E-4W-2
E-5
dFe (nmol L-1)
AOU (µmol kg-1)
0.0
0.1
0.2
0.3
0.4
0.5
0.6
0.7
0.8
0
20
40
60
80
100
120
140
160
180

Figure 8